

Journal of Materials Chemistry A

Accepted Manuscript



This is an *Accepted Manuscript*, which has been through the Royal Society of Chemistry peer review process and has been accepted for publication.

Accepted Manuscripts are published online shortly after acceptance, before technical editing, formatting and proof reading. Using this free service, authors can make their results available to the community, in citable form, before we publish the edited article. We will replace this *Accepted Manuscript* with the edited and formatted *Advance Article* as soon as it is available.

You can find more information about *Accepted Manuscripts* in the [Information for Authors](#).

Please note that technical editing may introduce minor changes to the text and/or graphics, which may alter content. The journal's standard [Terms & Conditions](#) and the [Ethical guidelines](#) still apply. In no event shall the Royal Society of Chemistry be held responsible for any errors or omissions in this *Accepted Manuscript* or any consequences arising from the use of any information it contains.

Strongly Coupled Thermal and Chemical Expansion in the Perovskite Oxide System $\text{Sr}(\text{Ti,Fe})\text{O}_{3-\alpha}$

Nicola H. Perry^{*a,b}, Jae Jin Kim^b, Sean R. Bishop^{a,b}, and Harry L. Tuller^{a,b}

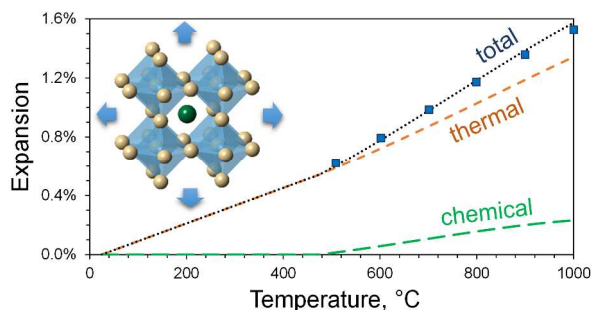
a. International Institute for Carbon-Neutral Energy Research (WPI-I²CNER), Kyushu University, Nishiku Fukuoka 819-0395, Japan

b. Department of Materials Science and Engineering, Massachusetts Institute of Technology, Cambridge, MA 02139, U.S.A.

* Corresponding author

Table of Contents Figure & Caption

To evaluate stability in energy conversion devices, thermal and chemical expansion coefficients (CTE, CCE) of $\text{Sr}(\text{Ti,Fe})\text{O}_{3-\alpha}$ were measured and deconvoluted for the first time, revealing an oxygen stoichiometry-dependent CTE and temperature-dependent CCE.



Abstract

The thermochemical expansion behavior of the mixed ionic and electronic conducting perovskite $\text{SrTi}_{1-x}\text{Fe}_x\text{O}_{3-\alpha}$ ($x = 0.05, 0.35$) was characterized to evaluate its potential stability in operating electrochemical devices and to quantify the coupling between oxygen stoichiometry changes and lattice expansion in this material. Changes in oxygen stoichiometry and dimensions of dense specimens were measured using thermogravimetric analysis and dilatometry, respectively, over a range of temperatures up to 1000 °C and oxygen partial pressures down to 10^{-4} atm, both under steady-state conditions and during thermal or oxygen activity excursions. The separate isothermal chemical expansion and iso-stoichiometric

thermal expansion contributions to overall expansion were thereby deconvoluted. For $x = 0.35$, the isothermal coefficient of chemical expansion (CCE) was found to increase with increasing temperature ($CCE = 3.0(3) \times 10^{-5} \times T + 1.9(2) \times 10^{-2}$; T is in $^{\circ}\text{C}$), while the iso-stoichiometric coefficient of thermal expansion (CTE) increased with increasing oxygen deficiency ($CTE = -3.00 \times 10^{-5} \times \delta + 1.44 \times 10^{-5}$, where $\delta = x/2 - \alpha$). From these relationships, and the measured change in oxygen stoichiometry upon heating, the overall thermo-chemical expansion during heating in air was successfully modeled. The effective size of a vacant anion site was also estimated as a function of temperature from the measured CCEs and found to be comparable to that of an occupied anion site at high temperatures (≥ 900 $^{\circ}\text{C}$). For $x = 0.05$, the changes in oxygen stoichiometry and expansion were smaller over a given temperature or oxygen partial pressure range, though the CCE appeared to be larger than for $x = 0.35$. Greater charge localization may be responsible for the higher CCE of the sample with the lower Fe content.

Introduction

The perovskite oxide system, $\text{Sr}(\text{Ti},\text{Fe})\text{O}_{3-\alpha}$ (STF), exhibits a number of attractive features, including a widely tailorable mixed ionic and electronic conductivity^{1,2}, fast oxygen surface exchange kinetics³, and a strong dependence of conductivity on oxygen partial pressure under lean burn conditions⁴. For these reasons, it has been investigated for application as a solid oxide fuel cell (SOFC) electrode^{5,6}, oxygen sensor^{1,7}, hydrocarbon gas sensor⁸, and oxygen permeation membrane⁹. The intermediate composition, $\text{SrTi}_{0.65}\text{Fe}_{0.35}\text{O}_{3-\alpha}$ (STF35), within the SrTiO_3 - SrFeO_3 solid solution, is characterized by a unique temperature-independent resistivity (over a certain temperature and oxygen partial pressure range)¹⁰, of interest in oxygen sensing and as an SOFC cathode because of its superior oxygen surface exchange kinetics, with little improvement for higher Fe concentrations¹¹. At higher Fe concentrations, ordering and phase instability may pose a problem, such as in oxygen-deficient $\text{SrFeO}_{3-\delta}$, which undergoes a transition to the ordered $\text{Sr}_2\text{Fe}_2\text{O}_5$ brownmillerite phase below ~ 800 - 900 $^{\circ}\text{C}$ (depending on oxygen partial pressure)^{12,13}. On the other hand, while substitution of Ti into SrFeO_3 stabilizes the

perovskite structure, it lowers both the ionic and electronic conductivity¹. In this work, as a consequence, we focus largely on the intermediate STF35 composition, with comparison made to the SrTi_{0.95}Fe_{0.05}O_{3- α} (STF5) composition.

In addition to the need to optimize the electrical and electrochemical properties of materials such as STF for the aforementioned devices, one must also consider their thermo-mechanical and chemo-mechanical properties to ensure stable device operation. For example, where STF is contacted by other materials and exposed to different temperatures and oxygen activities, thermal and chemical expansion may lead to large stresses^{14,15} and potentially mechanical failure through, e.g., cracking and delamination¹⁶. For high durability, it is desirable to match the coefficient of thermal expansion (CTE) with those of any adjacent materials and, particularly at high temperatures, to minimize the additional chemical expansion, i.e., expansion caused by redox-induced lattice dilation or contraction¹⁷. It is therefore important to characterize the thermal and chemical expansion behavior of candidate mixed ionic and electronic conductors both to ensure compatibility with other device components and to develop a better fundamental understanding of the factors controlling expansion. Additionally, quantification of chemical expansion is important for techniques that exploit this inherent chemo-mechanical coupling, such as determination of thin film oxygen non-stoichiometry by measure of the lattice parameter¹⁸, electrochemical strain microscopy¹⁹, and the curvature relaxation technique for determining oxygen incorporation rates²⁰.

Chemical expansion in the context of non-stoichiometric oxides refers to lattice dilation that accompanies a decrease in the oxygen content²¹; specifically, this type of expansion is termed “stoichiometric expansion.” Analogous to the coefficient of thermal expansion (CTE), the coefficient of chemical expansion (CCE, α_C) is phenomenologically defined as:

$$\alpha_C = \pm \varepsilon_C / \Delta\delta \quad (1)$$

where ϵ_C represents isothermal chemical expansion, $\Delta\delta$ indicates a change in oxygen stoichiometry (per formula unit), and the sign would be +ve for cases where δ represents oxygen deficiency (sub-stoichiometry) and -ve for cases where δ represents oxygen excess (super-stoichiometry) relative to the reference compound (as in the present work). It has been shown, in fluorite-structured oxides with multivalent cations such as CeO_2 , that, during reduction, the expansion of cations that lower their valence state outweighs the small contraction around the oxygen vacancies that also form²². (The smaller contraction around the oxygen vacancy is the net effect of cations relaxing outward and anions relaxing inward toward the vacancy. Others have also reported that the effective oxygen vacancy radius is significantly smaller than that of an oxygen ion in fluorites, and slightly smaller or similar to that of an oxygen ion in perovskites²³.) Similarly in the case of reduction of STF, the change in Fe radius as it reduces valence state from 4+ to 3+ (in oxidizing or cathodic conditions) and from 3+ to 2+ (in reducing or anodic conditions)²⁴, along with the change in oxygen concentration, is expected to play a significant role in chemical expansion. Defect chemical models developed by Rothschild *et al.*²⁵ and updated by Kuhn *et al.*²⁶, on the basis of electrical conductivity²⁵ and thermogravimetry data²⁶, can now predict the relevant defect concentrations as a function of temperature and oxygen partial pressure.

The above defect chemical model takes as the stoichiometric reference state $\text{SrTi}_{1-x}\text{Fe}_x\text{O}_{3-x/2}$, with 3+ the reference valence state for Fe given that the overall oxygen deficiency relative to SrTiO_3 always remains close to $x/2$, assuming predominantly trivalent Fe, with small excursions to further oxygen deficiency under reducing conditions and oxygen excess under oxidizing conditions^{25,26}. This reference state defines two types of anion sites: oxygen sites, with a concentration $(3-x/2)*[\text{STF}]$, and structural interstitial sites, with a concentration $(x/2)*[\text{STF}]$, where $[\text{STF}]$ is the volumetric concentration of STF formula units. The balance between further loss of oxygen, in the form of charged vacant oxygen sites ($V_{\text{O}}^{\bullet\bullet}$), and further addition of oxygen, in the form of charged occupied structural interstitial sites ($O_i^{\prime\prime}$), determines the oxygen non-stoichiometry of $\text{SrTi}_{1-x}\text{Fe}_x\text{O}_{3-(x/2)+\delta}$:

$$\delta = \frac{([O_i^{\prime\prime}] - [V_{\text{O}}^{\bullet\bullet}])}{[\text{STF}]} \quad (2)$$

where brackets indicate volumetric concentrations and superscripts denote relative charge, in Kröger-Vink notation. The temperature- and oxygen partial pressure-dependence of δ are described by the reduction, anion Frenkel, and intrinsic electronic defect formation reactions, with their thermally-activated equilibrium constants, and the charge neutrality equation^{25,26,27}. In the relatively oxidizing conditions used in the present study, the predominant electronic species is holes, and the electron concentration is negligible. If holes are fully localized on the multivalent Fe, then the concentration of holes is $p \approx [Fe^{4+}]$, whereas Fe^{3+} represents a neutral species. Correspondingly, the electroneutrality condition (ENC) becomes:

$$p \approx 2\delta[STF] \approx [Fe^{4+}] \quad (3)$$

In this case, slight decreases in oxygen content are accommodated by a corresponding decrease in the concentration of Fe^{4+} as it reduces to Fe^{3+} . If holes are delocalized, the relationship between oxygen content and Fe valence state may differ from eq. 3.

In this work the overall thermochemical expansion behaviors of STF35 and STF5 as a function of temperature and oxygen partial pressure are characterized. For STF35, the CCE in isothermal conditions and the CTE in iso-stoichiometric conditions are determined and applied, along with the defect chemical model, to model the total thermochemical expansion as a function of temperature in air. The defect model, in conjunction with an approach for relating lattice expansion to ionic radii in perovskites, are applied to estimate the expected CCE and effective size of a vacant anion site in STF35. The thermal and chemical expansion behavior of STF5 is then compared to those of STF35.

Results

The relative densities of the STF35 and STF5 pellets were 96.7 % and 96.4 %, respectively. These high relative densities are also apparent in the micrographs shown in figure 1. From the images in figure 1a and 1b, it was determined that the average grain size of the STF35 sample was $20.2 \pm 4.5 \mu\text{m}$, while that of the STF5 sample was $4.7 \pm 1.2 \mu\text{m}$. The higher Fe content corresponds to a larger average

grain size for the same sintering condition. The large grain sizes suggest that contributions from surfaces, grain boundaries, and sintering during the dilatometry measurements were negligible. Each sample (powders and pellets) exhibited a single phase cubic perovskite structure as shown by the X-ray diffraction patterns in figure 2. The ratios of Fe to (Fe+Ti) in the two pellets were 0.355 ± 0.003 and 0.061 ± 0.014 , which were close to the nominal values of 0.35 and 0.05.

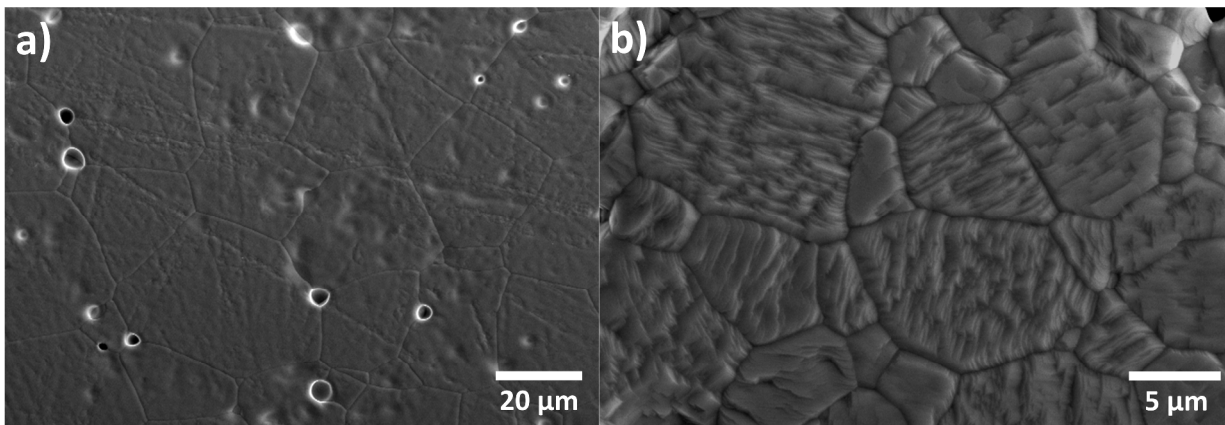


Figure 1. Microstructures of the polished and thermally etched STF35 (a) STF5 (b) specimens

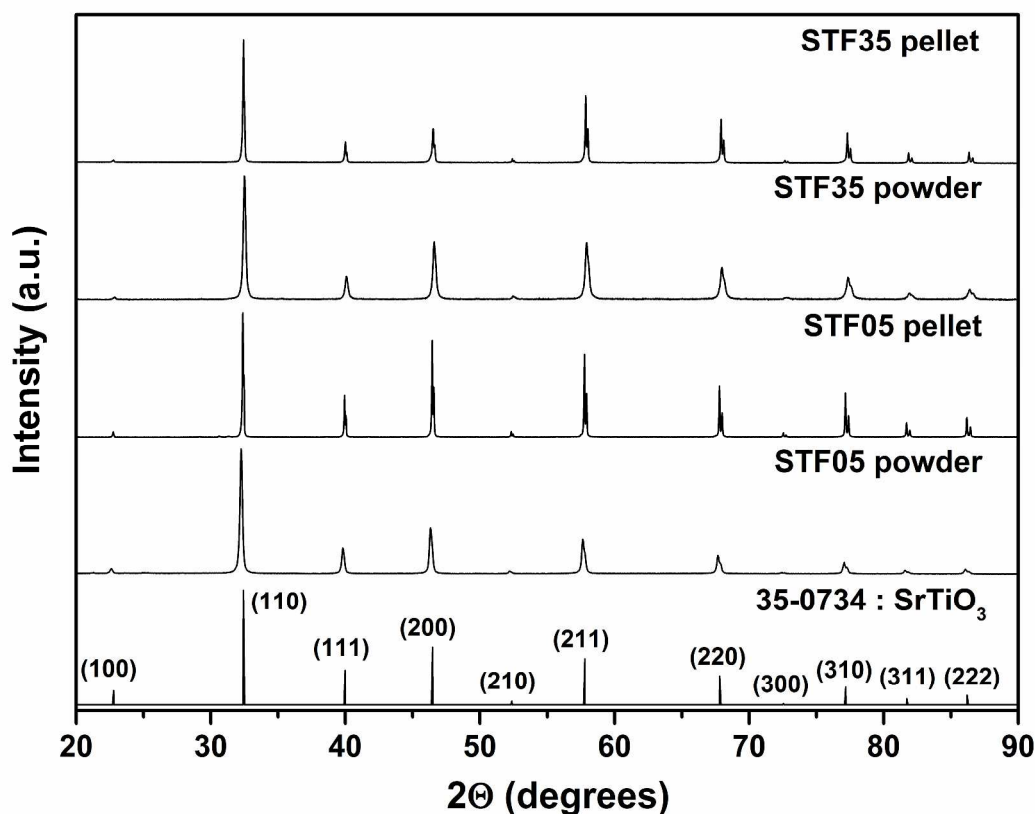


Figure 2. X-ray diffraction patterns of the STF35 and STF5 powders and pellets, showing peaks corresponding to the cubic perovskite phase.

The expansion of STF35 and STF5 measured in air as a function of temperature, during heating and cooling at 5 °C/min, is shown in figure 3a, referenced to the final room temperature values. Slight hysteresis is observed for both compositions, suggesting that the heating/cooling rate was insufficiently slow to obtain equilibrium or that there are unaccounted-for instrumental errors. For comparison, steady-state values of expansion for each composition are also shown for ~500 °C and above. It can be seen that the steady-state expansion values for STF35 are slightly larger than the values obtained during heating and cooling in the high temperature range (≥ 550 °C), while the steady-state vs. continuously measured values for STF5 are in reasonable agreement. In addition, the thermochemical expansion of STF35 is considerably larger than that of STF5, particularly in the high temperature range.

This expansion represents the sum of thermal and chemical expansion, as the value of δ (oxygen superstoichiometry vs. the reference state) decreases with increasing temperature²⁶. From the approximately linear behavior at low temperatures (50-400 °C), where the change in δ is assumed to be negligible (based on the expected slow surface exchange and bulk diffusivities at these temperatures vs. the heating/cooling rates), CTEs of 13.1 ppm / °C during heating and 12.3 ppm / °C during cooling were determined for STF35. For STF5 the low temperature (50-400 °C) CTEs were 10.9 ppm / °C during heating and 11.3 ppm / °C during cooling. As described later in this results section, the equilibrium CTE for STF35 was also calculated at high temperatures from an analysis of temperature-dependent expansion in iso-stoichiometric conditions, yielding values of CTE that were found to be dependent upon oxygen stoichiometry. That result suggests that the low temperature CTEs determined from figure 3 may be dependent on thermal history and the exact value of δ quenched into the samples. This dependence of CTE on δ contributes to its non-linear temperature dependence in figure 3. At high temperatures the upturn in expansion also includes the increased contribution from chemical expansion. The total expansion can be de-convoluted into the separate contributions from pure thermal expansion and pure chemical expansion at high temperatures:

$$\varepsilon_{TOT} = \varepsilon_C + \varepsilon_T \quad (4)$$

$$d\varepsilon_{TOT} = \frac{\partial \varepsilon}{\partial T, \delta} dT + \frac{\partial \varepsilon}{\partial \delta, T} d\delta = \alpha_T dT + \alpha_C d\delta \quad (5)$$

where α_T is the iso-stoichiometric CTE and α_C is the isothermal CCE. Expressions for α_T and α_C as a function of δ and temperature, respectively, were determined in the present work, as described later in the results section. These contributions are indicated by the curves in figure 3b, for STF35. For fitting purposes, the value of δ was considered “frozen in” below 475 °C, while steady-state values of δ measured in this work were used for higher temperatures.

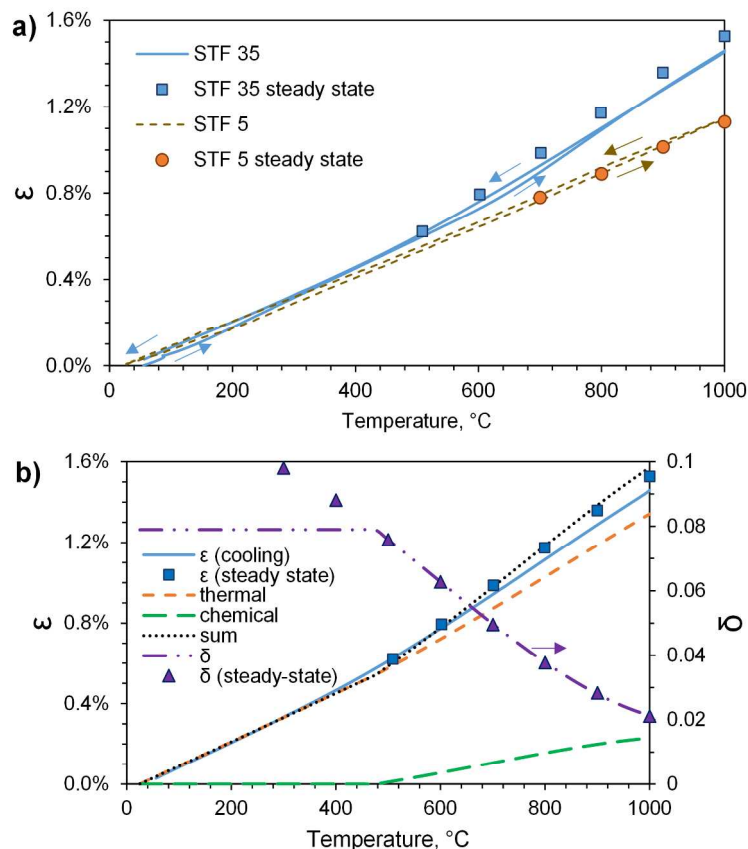


Figure 3. a) Expansion of STF35 and STF5 in air during heating and cooling at 5 °C/min and steady state expansion at various temperatures, measured by dilatometry, and corrected for instrument contributions. b) Calculated contributions from thermal and chemical expansion to the overall expansion of STF35 using high temperature CTE and CCE values and oxygen super-stoichiometry (δ) relative to the reference state, each determined in this work.

An example of isothermal chemical expansion at 700 °C is given in figure 4, which shows the measured expansion of STF35 and corresponding change in oxygen partial pressure as a function of time. The initial length of the sample, i.e., the reference point, is the length at 700 °C in 1 atm oxygen. One can observe from figure 4 that after each relatively rapid change in oxygen partial pressure, the sample takes time to reach its new equilibrium oxygen content and therefore to relax to its new length. This process is discussed further later.

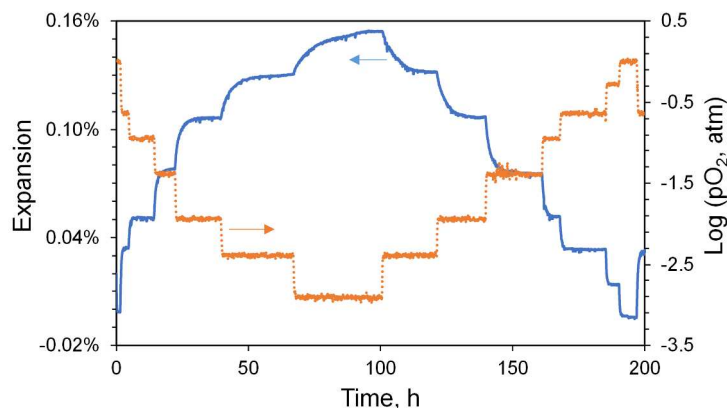


Figure 4. Expansion of STF35 and oxygen partial pressure changes recorded over time at 700 °C. The expansion values are referenced to the initial value (1 atm O₂ at 700 °C).

Figure 5a shows the equilibrium values of expansion as a function of oxygen partial pressure for each temperature measured, relative to the reference state of 27 °C and 0.21 atm O₂. As shown in the plot, the expansion values measured first upon reduction and then upon oxidation were nearly identical, indicating reversibility. This STF35 sample exhibits a gradual expansion upon exposure to more reducing conditions. The values of oxygen non-stoichiometry corresponding to the temperature and oxygen partial pressure conditions of this work²⁶ are shown in figure 5b, indicating the expected loss of oxygen from STF with decreasing pO₂. In order to facilitate a direct comparison of expansion and non-stoichiometry, i.e., extract the CCE using equation 1, the data in figure 5b were fit at each temperature with a quadratic expression to interpolate values of non-stoichiometry for the exact conditions where the expansion was measured. The result is shown for each temperature in figure 5c (again showing both the forward and reverse isothermal pO₂ sweeps, which are in good agreement). Recall from equation 2 that in this system higher values of δ correspond to higher oxygen contents, so in this case the absolute values of the negative slopes in fig 5c are the chemical expansion coefficients at each temperature.

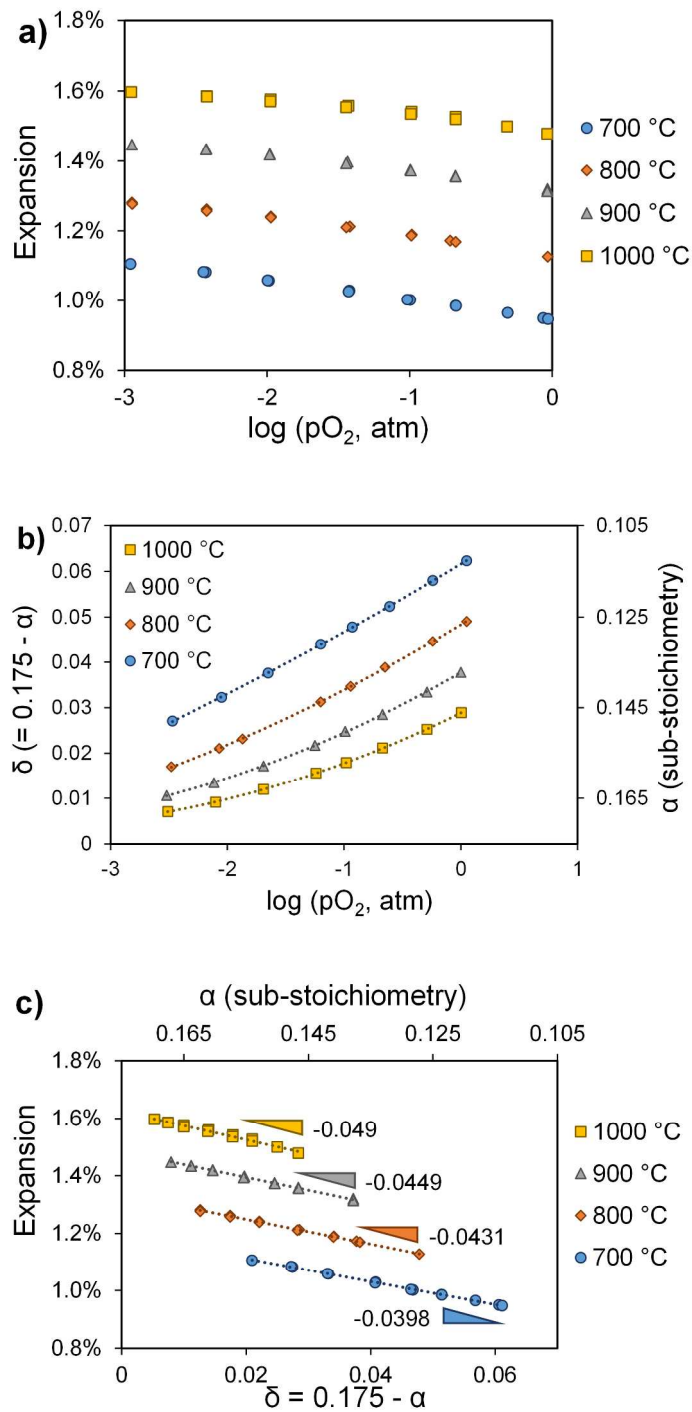


Figure 5. a) Expansion of STF35 (relative to 27 °C, 0.21 atm O_2) as a function of oxygen partial pressure at four temperatures. b) Absolute oxygen non-stoichiometry of STF35 as a function of oxygen partial pressure at four temperatures; data were taken from reference 26. Quadratic fits, used for interpolation, are also shown. Note the total oxygen content per formula unit is represented as $3 - (0.35/2) + \delta = 3 - \alpha$ for

the STF35 composition. c) Expansion of STF35 (relative to 27 °C, 0.21 atm O₂) as a function of oxygen non-stoichiometry at four temperatures. Slopes are indicated, with the magnitudes corresponding to the chemical expansion coefficients.

The chemical expansion coefficients for STF35 are 0.0398(3), 0.0431(5), 0.0449(6), and 0.049(1) at 700, 800, 900, and 1000 °C, respectively, where numbers in parentheses indicate the uncertainty on the last digit. The dependence of isothermal CCE (α_c) on temperature (in units of °C) in this high temperature range, which is to a first approximation linear ($R^2 = 0.98$), can be expressed as:

$$\alpha_c = 3.0(3) \times 10^{-5}T + 1.9(2) \times 10^{-2} \quad (6)$$

The linear dependence of isothermal expansion on oxygen non-stoichiometry in figure 5c enables fitting of the data to calculate expansion corresponding to a particular value of non-stoichiometry at each temperature. From such information it is possible to calculate iso-stoichiometric coefficients of thermal expansion (CTEs) in this high temperature range for comparison to the low temperature values. Figure 6 shows the resulting expansion vs. temperature for fixed values of oxygen non-stoichiometry, where the slopes are the CTEs. These slopes clearly depend on the oxygen content, with higher values of CTE corresponding to higher oxygen deficiencies (lower δ). For $\delta = 0, 0.02, 0.04,$ and 0.06 , the CTE values are 14.4(1), 13.8(2), 13.2(3), and 12.6(3) ppm/ °C, respectively, suggesting a linear dependence ($R^2=1$). The iso-stoichiometric CTE ($\alpha_T, ^\circ\text{C}^{-1}$) at high temperatures can thus be expressed as:

$$\alpha_T = -3.00 \times 10^{-5} \times \delta + 1.44 \times 10^{-5} \quad (7)$$

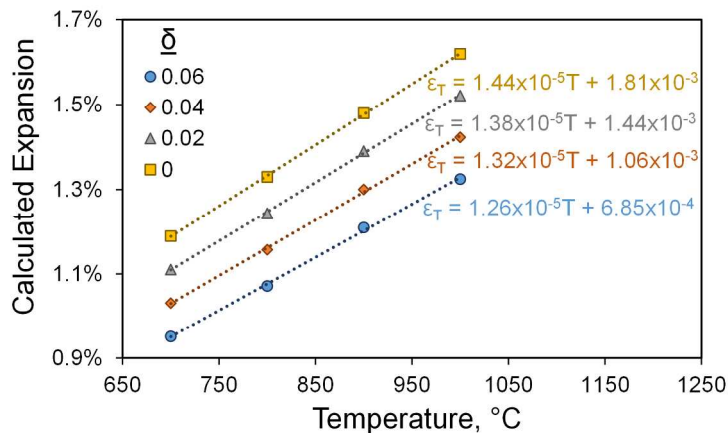


Figure 6. Iso-stoichiometric expansion of STF35 vs. temperature, interpolated/extrapolated from fig. 5c, relative to 27 °C at 0.21 atm O_2 .

For comparison to STF35, the isothermal chemical expansion behavior of STF5 is shown in figure 7. The chemical expansion as a function of oxygen partial pressure (a) was determined in the present work by dilatometry, whereas the estimated non-stoichiometry as a function of oxygen partial pressure, (b), was taken from ref. 26, for the similar composition $Sr_{0.9}Ba_{0.1}Ti_{0.95}Fe_{0.05}O_{3-a}$. In comparison to STF35, STF5 exhibited much smaller expansion and much smaller changes in oxygen stoichiometry upon exposure to lower oxygen pressures, as is expected from the lower concentration of the multivalent Fe cation. In contrast, the chemical expansion coefficients determined from the data in (a) and (b) are considerably larger than the values obtained for STF35, lying in the narrow range 0.065-0.067 for 700, 800, and 1000 °C (excluding the anomalous data at 900 °C, for which the CCE was 0.16). It should be noted that owing to the small magnitudes of both expansion and stoichiometry changes for this composition in the measured conditions, as well as the estimation of oxygen stoichiometry from a slightly different composition, there is more uncertainty in the values of chemical expansion coefficients for STF5 than for STF35.

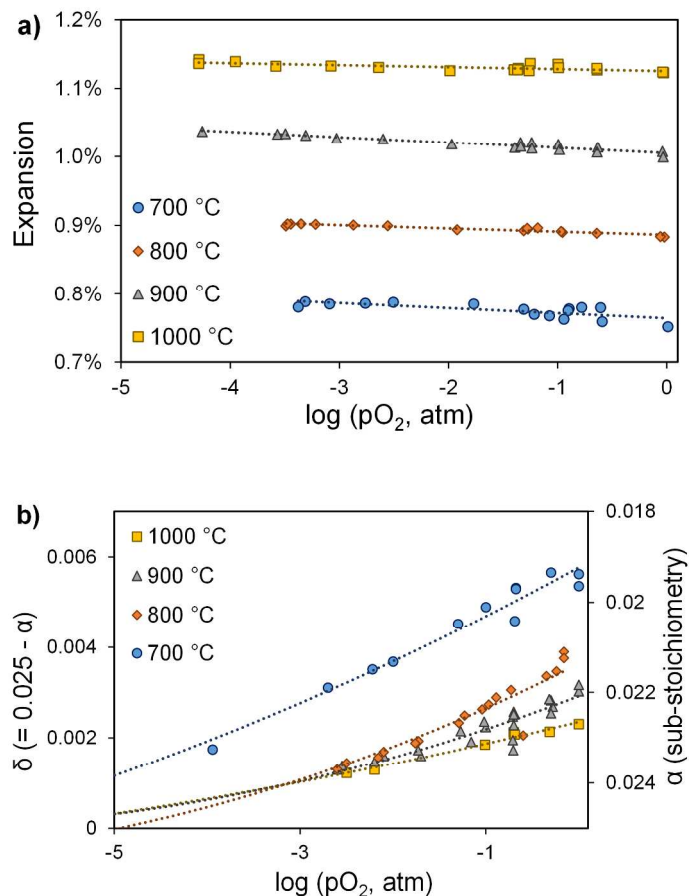


Figure 7. (a) Expansion of STF5 (relative to 27 °C, 0.21 atm O_2) as a function of oxygen partial pressure at four temperatures. (b) Oxygen stoichiometry as a function of oxygen partial pressure at four temperatures for the similar composition $Sr_{0.9}Ba_{0.1}Ti_{0.95}Fe_{0.05}O_{3-0.05/2+\delta}$, from ref. 26.

Discussion

In figure 3a it can be seen that the expansion/contraction during heating/cooling at 5 °C/min does not reach the steady-state values for STF35, which is consistent with the finite relaxation times observed for this composition's chemical expansion in figure 4, discussed below. The larger discrepancy (and larger expansion) for STF35 vs. STF5 is consistent with the larger amount of overall chemical expansion and larger stoichiometry changes upon heating associated with higher concentration of multivalent Fe. Chemical expansion contributes less to the overall thermo-chemical expansion in air for STF5, resulting in less curvature in the expansion vs. temperature plot and less discrepancy between steady-state values

and values measured during heating or cooling. In figure 3b the thermo-chemical expansion model for STF35, based on equations 5-7, is in good agreement with the steady-state data at high temperatures. The slight deviation of the model vs. the measurements during cooling in the intermediate temperature range may indicate that equations 6-7 are only valid in the high temperature range in which they were developed, 700-1000 °C, and/or that the oxygen stoichiometry in the sample during cooling deviates slightly from the steady state values shown in figure 3b at lower temperatures. For the low temperature data, the value of δ that best fits the data is the steady-state value for ~450-550 °C, suggesting frozen-in non-stoichiometry at low temperatures instead of further oxidation as seen in steady-state measurements.

It is observed from figure 4 that the relaxation times of STF35 upon changing oxygen partial pressure are faster in the higher oxygen partial pressure conditions. Based on an estimation of the critical length for STF35 of 200 μm at 700 °C²⁸, the relaxation behavior of this highly dense bulk sample is expected to be limited more by bulk chemical diffusion than by surface exchange kinetics. The slower kinetics at lower oxygen partial pressures may reflect the lower hole concentrations in these conditions, leading to a lower chemical diffusivity. An analysis of the expansion relaxation kinetics as a function of temperature, oxygen partial pressure, and composition is ongoing and will be reported in a later publication.

Three features are apparent from figure 5c. First, the magnitudes of the slopes (chemical expansion coefficients) are consistent with measured values for other mixed ionic and electronic conductors with the perovskite structure. The CCE values of STF35, ranging from 0.0398-0.049 at 700-1000 °C, fall within the reported range from 0.02 to 0.06 for perovskites including (La,Sr)CoO_{3- α} , (La,Sr)FeO_{3- α} , (La,Sr)(Fe,Ga)O_{3- α} , (La,Sr)(Co,Fe)O_{3- α} , (Ba,Sr)(Co,Fe)O_{3- α} , (La,Sr)MnO_{3- α} , and (La,Sr)CrO_{3- α} (see ref 21 and references therein), although the values in the present work lie above the majority of the reported values. (The CCEs are still lower than those reported for Ce-based fluorite-structured oxides, typically ~0.1²¹.) The many factors controlling chemical expansion in perovskites make generalizations difficult, but Frade²⁹ has noted a trend in some cases towards increasing CCE with

increasing perovskite tolerance factor (t). STF35 has a tolerance factor of 0.995 (calculated for all Fe^{3+} , all high spin and neglecting oxygen vacancies), which should place it towards the upper end of perovskite CCE values by that relationship. It is possible that radius expansion is more directly translated into lattice parameter expansion in the highly symmetric ($t \rightarrow 1$) perovskites, compared to the distorted perovskites ($t < 1$ or $t > 1$), where radius expansion may change the symmetry through octahedral tilting or distortion, leading to smaller, anisotropic lattice expansion³⁰. On the other hand, on the basis of B site ionic radii alone, one might expect Fe-containing perovskites to exhibit *smaller* CCE values than perovskites containing other multivalent cations, since the radius change for $\text{Fe}^{4+/3+}$ (~10%) is less than those of $\text{Co}^{4+/3+}$ (~15%), $\text{Cr}^{4+/3+}$ (~12%), and $\text{Ni}^{3+/2+}$ (~15%), assuming 6-fold coordination and the high spin state for the 3+ cation in each case. Departure from purely ionic bonding (charge delocalization), changes in B-site coordination (effectively changing the cation radius), changes in spin state, and/or an overriding role of crystal symmetry changes may be responsible for the different behavior observed in experiments. Indeed, in previous work^{30,31,32}, we have shown that localization of charge on the multivalent cation undergoing expansion can lead to a higher chemical expansion coefficient. Fe-bearing perovskites exhibit relatively low hole mobilities, consistent with charge localization, although both polaronic (hopping) conduction³³ and metallic conduction²⁵ have been suggested to take place at elevated temperatures. Thus the question of whether holes are fully localized on Fe remains open at present.

Considering further the charge-localized case, where the change in Fe valence state is accommodated by a change in oxygen stoichiometry as described in the introduction, it is possible to estimate the expected CCE for STF35. The lattice parameter change for the fully oxidized (super-oxidized) case ($[\text{Fe}^{4+}]/[\text{STF}] = 0.35$; $\delta=0.17$) vs. a more reduced condition (the stoichiometric reference state, i.e., $[\text{Fe}^{3+}]/[\text{STF}]=0.35$; $\delta=0$) may be calculated using a recently developed approach to predict lattice parameters (a) of perovskites^{30,34} using Shannon's ionic radii for the A-site, B-site, and oxygen ions³⁵ (note that ionic bonding is assumed for this estimate):

$$a = \frac{A}{\sqrt{2}}(r_A + r_X) + B(r_B + r_X) + C \quad (8)$$

Here, A, B, and C are parameters determined from fitting lattice parameter values for many perovskites ($A = 0.816$, $B = 1.437$, and $C = -0.609$)³⁴, while r_A , r_B , and r_X are the 12-coordinate A-site, 6-coordinate B-site, and 6-coordinate anion radii, respectively. Assuming that the Fe^{3+} is in the high spin state, and assuming the oxygen vacancy radius is similar to the oxygen ion radius, the expansion upon reduction, $(a - a_0)/a_0$, is calculated as $\sim 0.8\%$; dividing by the known $\Delta\delta$ yields a CCE of ~ 0.046 . This value may be an overestimate, given the use of the Shannon radii and the assumption that a vacant oxygen (or “structural interstitial” site) has the same radius as an occupied oxygen (or “structural interstitial” site). The slightly smaller CCE values observed experimentally at lower temperatures suggest that the holes may not be completely localized and/or that the vacant anion site has a smaller radius than an occupied anion site under those conditions. (An even smaller approximate experimental value for CCE of ~ 0.03 can be determined from room temperature X-ray diffraction data for nominally fully oxidized and fully reduced samples of $\text{SrTi}_{0.7}\text{Fe}_{0.3}\text{O}_{3-a}$ ³⁶.) However the estimated CCE is in good agreement with the measured values at higher temperatures, suggesting that the assumptions of the calculation may be reasonable under these conditions. Using this same model³⁴ it is possible to estimate the effective vacant anion site radius (r_V , weighted average of vacant oxygen sites and vacant structural interstitial sites) from the measured CCE values:

$$r_V = \frac{3\alpha_V a_0}{\left(\frac{A}{\sqrt{2}} + B\right)} + r_O \quad (9)$$

$$\alpha_V = \alpha_C - \frac{2\alpha_B}{z} \quad (10)$$

$$\alpha_B = \frac{B}{a_0} (r_{B^{sub}} - r_{B^{host}}) \quad (11)$$

Here, a_0 is the initial lattice parameter, r_O is the oxygen ion radius, α_C is the isothermal CCE, z represents the fraction of the B-site occupied by the multivalent cation (e.g., 0.35 for STF35), $r_{B^{sub}}$ is the final average radius of the B-site cation (in this case averaged for Fe^{3+} and Ti^{4+}), and $r_{B^{host}}$ is the initial average radius of the B-site cation (in this case averaged for Fe^{4+} and Ti^{4+}). Further details and a

derivation of these equations, which again assume ionic bonding (therefore localized charges) and high spin Fe^{3+} , are given in ref. 34. For 700, 800, 900, and 1000 °C, the effective vacant anion site radii in STF35 are determined to be 1.38, 1.39, 1.41 and 1.43 Å, respectively. These values are comparable to the ionic radius of an occupied anion site (1.40 Å), consistent with other reports^{23,34} on perovskites but larger than the estimated oxygen vacancy radii in fluorite-structured oxides²². Note that these values represent an average over all unoccupied anion sites, whereas local variations, e.g., different radii for the structurally non-equivalent²⁵ vacant interstitial site (V_i^x) vs. vacant oxygen site ($V_o^{\cdot\cdot}$), are in theory possible if local coordination environments of anion sites differ.

Second, the chemical expansion appears to exhibit a linear dependence upon oxygen non-stoichiometry at all temperatures. Linear behavior suggests that the local defect (and crystal) structure is not changing appreciably over the studied oxygen activity range. A non-linear dependence of chemical expansion on non-stoichiometry has previously been attributed to the presence of defect association in fluorite structured oxides^{37,38}, since the concentration of associates depended upon the non-stoichiometry. In those studies, defect association led to a decrease in apparent CCE with increasing oxygen deficiency in one case and an increase in the other. In contrast, other work proposing the presence of defect association at low temperatures (owing to the temperature dependence of the chemical expansion coefficient) reported a linear dependence of expansion on non-stoichiometry³⁹. Thus it appears that in the present case the presence of short-range ordering cannot be ruled out on the basis of the linear behavior. In fact, short-range ordering/ association of oxygen vacancies and Fe^{3+} ions has been reported in STF^{2,40,41,42}, and it is possible that non-linear chemical expansion behavior might be observed over a wider range of oxygen stoichiometries than were studied in this work.

Third, the chemical expansion coefficient is dependent upon temperature, monotonically increasing 24% from 700 to 1000 °C. Again it is possible that disordering of defect associates upon increasing the temperature could contribute to this trend³⁹. Both the cation and anion vacancy radii may be expected to be different in a nearest-neighbor, associated situation vs. an unassociated case, owing to

the influence of cation environment on oxygen vacancy radius⁴³ and of coordination number on cation radius³⁵, which could lead to temperature-dependent chemical expansion coefficients. One alternative explanation is that with increasing temperature, bonds extend and become weaker, enabling even larger expansions upon reduction. Another possibility is that the spin state of Fe³⁺ may increase in the temperature range of this study, leading to a larger Fe³⁺ radius³⁵ at higher temperatures and increased expansion upon reduction from Fe⁴⁺ to Fe³⁺. Significant temperature dependence of the chemical expansion coefficient has been observed previously for La_{0.3}Sr_{0.7}FeO_{3-δ} and La_{0.3}Sr_{0.7}Fe_{0.6}Ga_{0.4}O_{3-δ} perovskites⁴⁴.

From figure 6 it may be noted that most of the CTE values (absent of chemical expansion contributions) obtained in this stoichiometry ($\delta < 0.06$) and temperature range (700-1000 °C) are larger than those measured by dilatometry in the low temperature range (50-400 °C); however, the oxygen content at lower temperatures is expected to be higher (depending on thermal history), and CTEs are well known to non-linearly increase with temperature. Extrapolation of the measured oxygen non-stoichiometry of STF35 in air from higher temperatures down to room temperature indicates that in equilibrium, in air, the sample should come close to full (super-)oxidation, $\delta = 0.175$. In the present case a smaller value of δ at low temperatures indicates that the sample is in a non-equilibrium state, with the non-stoichiometry reflecting a value quenched in from a higher temperature (450-550 °C), as discussed above. Such a conclusion is also consistent with the fitting in figure 3b. Thus the high temperature values of CTE (12.6 – 14.4 ppm/ °C) are consistent with the generally smaller values (12.3-13.1 ppm/ °C) measured at lower temperatures. Previous studies have also noted a dependence of iso-stoichiometric CTE on oxygen non-stoichiometry^{44,45}. In such cases the increase in CTE with decreasing oxygen content has been attributed to a decrease of lattice binding energy⁴⁴, increase in atomic vibration anharmonicity⁴⁵, or decrease in Pauling bond strength, owing to the lower valence state and coordination of the B-site cation⁴⁵. While a number of mechanisms are possible, the overall result is that higher oxygen deficiencies yield higher CTEs, and similarly, higher temperatures yield higher CTEs.

In figure 7 the smaller magnitudes of expansion and oxygen stoichiometry changes observed for STF5 vs. STF35 are expected on the basis of the different Fe concentrations. The apparently larger CCEs for STF5 vs. STF35 are consistent with similar results obtained for another perovskite, (La,Sr)(Ga,Ni)O_{3-δ}, in which smaller concentrations of Ni (0.05 and 0.1 vs. 0.5 per formula unit) were associated with a higher degree of charge localization on the multivalent cation and correspondingly higher CCEs³⁰. Indeed, the measured CCEs for STF5 are in reasonable agreement with the calculated CCE for the charge localized case discussed above. The possibility of greater charge localization for smaller Fe contents is also consistent with the reported electrical conductivity behavior. Upon increasing the Fe content, x, in Sr_{0.9}Ba_{0.1}Ti_{1-x}Fe_xO_{3-x/2+δ} from 0.05 to 0.35, the hole concentration increases by a factor of ~10, based on reported values of δ²⁶ in oxidizing conditions and the charge neutrality condition in eq. 3. By contrast, the p-type electronic conductivity increases two orders of magnitude¹, indicating a significant increase in hole mobility (by a factor of ~10) as the Fe content increases from 0.05 to 0.35. (The presence of a small amount of Ba on the A-site is not expected to significantly affect this trend compared to pure STF.)

Experimental Approach

Single-phase SrTi_{0.65}Fe_{0.35}O_{2.825+δ} (STF35) and SrTi_{0.95}Fe_{0.05}O_{2.975+δ} (STF5) powders were synthesized by the Pechini-type polymer complex method^{26,46}. First, Ti[OCH(CH₃)₂]₄ was dripped into ethylene glycol (EG), followed by adding citric acid (CA) to form a metal-organic complex. The resultant solution was clear without precipitation. After that, the respective stoichiometric ratio of Sr(NO₃)₂ and Fe(NO₃)₃•9H₂O and 500 ml of distilled water were added. The mole ratio of Sr²⁺ ions, EG and CA was 1:32:4. The resultant mixtures were stirred at 90 °C until a dry gel formed through polyesterification between EG and CA. After drying at 110 °C for 12 hours, the as-obtained powders were pre-fired at 500 °C for 2 hours and then fully calcined at 950 °C for 7 hours in air. After sieving through a 75 μm-sized sieve, the powders were pressed into pellets (weight of approximately 6 g) by applying 292 MPa of uniaxial pressure, and then sintered at 1650 °C for 12 hours in air. The relative densities of the pellets

were measured by the Archimedes method. For dilatometry measurements, the pellets were cut into bars (~ 20 mm x 4 mm x 4 mm).

The phase purity of the powders and the pellets was examined by X-ray diffraction (Cu K α , 45 kV and 40 mA, PANalytical X'Pert Pro Multipurpose Diffractometer) at room temperature in air. The chemical compositions of the pellets were confirmed by wavelength dispersive X-ray spectroscopy (JEOL-JXA-8200 Superprobe). The standard used for Sr, Ti, and O was SrTiO₃, and the one for Fe was Fe₂O₃. After polishing and thermal etching at 1400 °C for 30 min (STF35) or 1600 °C for 1 h (STF5) in air, the microstructures of the pellets were investigated by scanning electron microscopy (FEI/Philips XL30 FEG ESEM).

Thermo-chemical expansion of the STF5 and STF35 bar-shaped specimens was measured in air using a custom-built Al₂O₃ push-rod dilatometer and a Linseis push-rod dilatometer in the temperature range 60-1000 °C during heating and cooling at 5 °C/min. The data were corrected for instrument contributions by measuring a polycrystalline Al₂O₃ reference sample of identical length over the same temperature profile and using reported thermal expansion data⁴⁷ for polycrystalline Al₂O₃ to determine the instrument contribution. Similarly, steady state thermo-chemical expansion of STF35 and STF5 after holding the samples at various temperatures in air (during heating) was measured with the custom-built push-rod dilatometer. These data were similarly corrected for the instrument contribution by measuring an Al₂O₃ reference sample at the same steady-state temperature conditions. In this work, expansion (ϵ) is defined as:

$$\epsilon = \Delta l/l_0 = (p - p_{ref})/l_0 \quad (12)$$

where Δl is the change in sample length determined from the dilatometer position (p) relative to a reference point (p_{ref} , defined later) and l_0 is the initial length measured at room temperature in air (20 mm in this case). Using l_0 instead of the actual sample reference length where the reference is defined (at p_{ref}) results in very small error in the expansion calculation ($< \sim 1\%$).

In order to model the aforementioned thermo-chemical expansion of STF35 in air, the steady-state oxygen non-stoichiometry of STF35 was determined by thermogravimetry, after holding at different temperatures (300-1000 °C, in 100 °C increments) in 0.21 atm O₂. Sample mass was measured by suspending the sample from an XP6 microbalance (Mettler-Toledo K.K., Tokyo, Japan) with Pt wire in an atmosphere-controlled tube furnace with a gas flow rate of 100 sccm. Oxygen non-stoichiometry changes were determined from mass changes using the following equation:

$$\Delta\delta = \frac{\text{mol O gained}}{\text{mol STF}} = \frac{(m - m_{ref})/M_O}{\text{mol STF}} \quad (13)$$

where $m - m_{ref}$ is the sample's mass change vs. the reference point (in g), M_O is the mass of a mole of atomic oxygen, and "mol STF" is the number of moles of $\text{SrTi}_{1-x}\text{Fe}_x\text{O}_{3-x/2+\delta}$ in the specimen, estimated from the initial sample mass at room temperature. The absolute stoichiometry at 1000 °C in 0.21 atm O₂ was assumed to be equal to that reported for this composition under the same conditions in ref. 26, and other values were calculated from this reference point. The high temperature isothermal CCE and iso-stoichiometric CTE values, determined as described below and in the results section, were also used to model the thermo-chemical expansion behavior.

Determination of isothermal chemical expansion (and indirectly iso-stoichiometric thermal expansion; see results section) was accomplished by separate measurements of 1) oxygen non-stoichiometry at different oxygen partial pressures by thermogravimetric analysis and 2) uniaxial expansion over the same range of oxygen partial pressures. The thermogravimetric analysis from 600-1000 °C was performed previously, as described in ref. 26. Isothermal uniaxial expansion vs. oxygen partial pressure was measured at 700, 800, 900, and 1000 °C in the custom-built push-rod dilatometer. Oxygen partial pressure was controlled with mass flow controllers and N₂ / O₂ gas mixtures (from pure N₂ to pure O₂) and monitored *in situ* with a Y₂O₃-stabilized ZrO₂ Nernst-type electromotive force sensor; the gas flow rate was held constant at 200 sccm. Measurements were made initially in decreasing steps of oxygen partial pressure and then repeated in increasing partial pressure increments to verify reversibility.

Continuous monitoring of sample expansion enabled determination of the equilibrium value and time taken to reach equilibrium. Sample temperature was monitored with an S-type thermocouple. Data were corrected for temperature-dependent instrument contributions via measurements of an Al₂O₃ standard, as described previously.

Conclusions

The strongly coupled thermal and chemical expansion behaviors of SrTi_{1-x}Fe_xO_{3-x/2+δ} (x = 0.05, 0.35) were studied by dilatometry and thermogravimetric analysis up to 1000 °C and down to an oxygen partial pressure of 10⁻⁴ atm. For STF35 the isothermal coefficient of chemical expansion (pO₂ = 10⁻³ to 1 atm) was found to increase with increasing temperature and ranged from ~0.04 to ~0.05 from 700 to 1000 °C. These CCE values fall near the top of the range for CCEs of other mixed ionic and electronic conductors with perovskite structures but are lower than those of Ce-based fluorite-structured oxides. The effective radius of an unoccupied anion site, calculated from these measured high temperature CCE values, was also found to increase with temperature, being comparable to that of an oxygen ion at high temperatures. The iso-stoichiometric coefficient of thermal expansion for STF35, determined from chemical expansion data at different temperatures, depended linearly on oxygen content. Values of CTE ranged from 12.6 to 14.4 ppm/ °C for δ=0.06 to δ=0 at 700-1000 °C. The measured CTE at 50-400 °C was 12.3-13.1 ppm/ °C, which is reasonable considering the expected higher oxygen content at lower temperatures. For STF5, the magnitude of the chemical expansion (and thus overall thermochemical expansion) over a given oxygen partial pressure or temperature range was smaller, owing to the lower multivalent cation concentration. The apparent low temperature CTE was also slightly smaller, at 10.9-11.3 ppm/ °C. By contrast, the high temperature CCEs of ~0.07 appeared to be higher than those of STF35, though owing to the almost negligibly small changes in oxygen content and expansion over the measured oxygen partial pressure range for STF5, larger uncertainty exists in the derived CCE values. The higher CCE, coexisting with lower hole mobility, for the lower Fe content is consistent with previous reports of increased CCE with increased charge localization.

Acknowledgments

NHP gratefully acknowledges support from JSPS KAKENHI grant number 25820334. NHP and SRB recognize partial support from I2CNER, supported by the World Premier International Research Center Initiative (WPI), MEXT, Japan. JJK and HLT thank the Basic Energy Sciences, U.S. Department of Energy under award DE-SC0002633 for research support. HLT acknowledges support from the Progress-100 program for MIT-Kyushu University collaboration.

- ¹ C. Heilig, "Characterisierung der elektrischen eigenschaften von Sr(Ti,Fe)O₃ im hinblick auf die anwendung in sauerstoffsensoren (Characterization of the electrical properties of Sr(Ti,Fe)O₃ in view of an application as oxygen sensors)," Diploma Thesis (in German), Universität Karlsruhe (TH), Karlsruhe, Germany, 1996.
- ² S. Steinsvik, R. Bugge, J. Gjønnnes, J. Taftø, and T. Norby, "The defect structure of SrTi_{1-x}Fe_xO_{3-y} (x=0-0.8) investigated by electrical conductivity measurements and electron energy loss spectroscopy (EELS)," *Journal of Physics and Chemistry of Solids* 58 [6] (1997) 969-976
- ³ T. Bieger, J. Maier, and R. Waser, "Kinetics of oxygen incorporation in SrTiO₃ (Fe-doped) – an optical investigation," *Sensors and Actuators B – Chemical* 7 [1-3] (1992) 763-768
- ⁴ H.L. Tuller, "Materials for high temperature electrochemical applications: automotive sensors, catalysts and traps," *Sensors & Actuators B*, 187 (2013) 106-110.
- ⁵ D.P. Fagg, V.V. Kharton, A.V. Kovalevsky, A.P. Viskup, E.N. Naumovich, and J.R. Frade, "The stability and mixed conductivity in La and Fe doped SrTiO₃ in the search for potential SOFC anode materials," *Journal of the European Ceramic Society* 21 [10-11] (2001) 1831-1835
- ⁶ J.C. Ruiz-Morales, J. Canales-Vazquez, H. Lincke, J. Pena-Martinez, D. Marrero-Lopez, D. Perez-Coll, J.T.S. Irvine, and P. Nunez, "Potential electrode materials for symmetrical solid oxide fuel cells," *Boletin de la Sociedad Espanola de Ceramica y Vidrio* 47 [4] (2008) 183-188
- ⁷ W. Menesklou, H.J. Schreiner, K.H. Hardtl, and E. Ivers-Tiffée, "High temperature oxygen sensors based on doped SrTiO₃," *Sensors and Actuators B – Chemical* 59 [2-3] (1999) 184-189
- ⁸ K. Sahrner, R. Moos, M. Matam, and M. Post, "Thick and thin film p-type conducting perovskite hydrocarbon sensors – a comparative study," *Proceedings of the IEEE Sensors 2003*, Vols 1 and 2 (2003) 926-931
- ⁹ J.R. Jurado, F.M. Figueiredo, B. Gharbage, and J.R. Frade, "Electrochemical permeability of Sr_{0.7}(Ti,Fe)O_{3-δ} materials" *Solid State Ionics* 118 [1-2] (1999) 89-97
- ¹⁰ W. Menesklou, H.J. Schreiner, R. Moos, K.H. Hardtl, E. Ivers-Tiffée, "Sr(Ti,Fe)O₃: Material for a temperature independent resistive oxygen sensor," *Materials of Smart Systems III (Book series: Materials Research Society Symposium Proceedings)* 604 (2000) 305-310
- ¹¹ W.C. Jung and H.L. Tuller, "A new model describing solid oxide fuel cell cathode kinetics: model thin film SrTi_{1-x}Fe_xO_{3-δ} mixed conducting oxides – a case study," *Advanced Energy Materials* 1 (2011) 1184-1191
- ¹² J.-C. Grenier, N. Ea, M. Pouchard, and P. Hagenmuller, "Structural transitions at high temperature in Sr₂Fe₂O₅" *Journal of Solid State Chemistry* 58 (1985) 243-252
- ¹³ M. Schmidt and S.J. Campbell, "Crystal and magnetic structures of Sr₂Fe₂O₅ at elevated temperature," *Journal of Solid State Chemistry* 156 (2001) 292-304
- ¹⁴ A. Atkinson, "Chemically-induced stresses in gadolinium-doped ceria solid oxide fuel cell electrolytes," *Solid State Ionics* 95 [3-4] (1997) 249-258
- ¹⁵ R. Krishnamurthy and B.W. Sheldon, "Stresses due to oxygen potential gradients in non-stoichiometric oxides," *Acta Materialia* 52 [7] (2004) 1807-1822
- ¹⁶ K. Sato, T. Hashida, K. Yashiro, H. Yugami, T. Kawada, and J. Mizusaki, "Mechanical damage evaluation of solid oxide fuel cells unders simulated operating conditions," *Journal of the Ceramic Society of Japan* 113 [1320] (2005) 562-564
- ¹⁷ X.Y. Chen, J.S. Yu, and S.B. Adler, "Thermal and chemical expansion of Sr-doped lanthanum cobalt oxide (La_{1-x}Sr_xCoO_{3-δ})," *Chemistry of Materials* 17 [17] (2005) 4537-4546

- ¹⁸ M.D. Biegalski, E. Crumlin, A. Balianinov, E. Mutoro, Y. Shao-Horn, and S.V. Kalinin, "In situ examination of oxygen non-stoichiometry in $\text{La}_{0.80}\text{Sr}_{0.20}\text{CoO}_{3-\delta}$ thin films at intermediate and low temperatures by X-ray diffraction," *Appl. Phys. Lett.*, 104, 161910 (2014)
- ¹⁹ S. Kalinin, N. Balke, S. Jesse, A. Tselev, A. Kumar, T.M. Arruda, S. Guo, and R. Proksch, "Li-ion dynamics and reactivity on the nanoscale," *Materials Today* 14 [11] (2011) 548-558
- ²⁰ Q. Yang, T.E. Burye, R.R. Lunt, J.D. Nicholas, "In situ oxygen surface exchange coefficient measurements on lanthanum strontium ferrite thin films via the curvature relaxation method," *Solid State Ionics* 249-250 (2013) 123-128
- ²¹ S.R. Bishop, D. Marrocchelli, C. Chatzichristodoulou, N.H. Perry, M.B. Mogensen, H.L. Tuller, and E.D. Wachsman, "Chemical expansion: Implications for electrochemical energy storage and conversion devices," *Annual Review of Materials Research*, 44 (2014) 205-239
- ²² D. Marrocchelli, S.R. Bishop, H.L. Tuller, and B. Yildiz, "Understanding chemical expansion in non-stoichiometric oxides: ceria and zirconia case studies," *Advanced Functional Materials* 22 [9] (2012) 1958-1965
- ²³ C. Chatzichristodoulou, P. Norby, P. V. Hendriksen, and Mogens B. Mogensen, "Size of oxide vacancies in fluorite and perovskite structured oxides," *J. Electroceram.* (Online, April 2014) DOI 10.1007/s10832-014-9916-2
- ²⁴ H.-J. Hagemann, "Akzeptorionen in BaTiO_3 und SrTiO_3 und ihre auswirkung auf die eigenschaften von titanatkeramiken" thesis, Aachen (1980)
- ²⁵ A. Rothschild, W. Menesklou, H.L. Tuller, and E. Ivers-Tiffée, "Electronic structure, defect chemistry, and transport properties of $\text{SrTi}_{1-x}\text{Fe}_x\text{O}_{3-y}$ solid solutions," *Chem. Mater.* 18 (2006) 3651-3659
- ²⁶ M. Kuhn, J.J. Kim, S.R. Bishop, H.L. Tuller, "Oxygen nonstoichiometry and defect chemistry of perovskite-structured $\text{Ba}_x\text{Sr}_{1-x}\text{Ti}_{1-y}\text{Fe}_y\text{O}_{3-y/2+\delta}$ solid solutions" *Chem. Mater.* 25 [15] (2013) 2970-2975
- ²⁷ N.H. Perry, D. Pergolesi, S.R. Bishop, and H.L. Tuller, "Defect chemistry and surface oxygen exchange kinetics of La-doped $\text{Sr}(\text{Ti},\text{Fe})\text{O}_{3-\alpha}$ in oxygen-rich atmospheres" *Solid State Ionics* (Online, October 2014) DOI 10.1016/j.ssi.2014.09.013
- ²⁸ W.C. Jung, "A new model describing cathode kinetics in solid oxide fuel cell: model thin film $\text{SrTi}_{1-x}\text{Fe}_x\text{O}_{3-\delta}$ mixed conducting oxides – a case study," PhD Thesis, MIT (2010)
- ²⁹ J.R. Frade, "Challenges imposed by thermochemical expansion of solid state electrochemical materials," p. 95 in *Solid Oxide Fuels Cells: Facts and Figures*, J.T.S. Irvine and P. Connor, eds., Springer (2013)
- ³⁰ N.H. Perry, S.R. Bishop, and H.L. Tuller, "Tailoring chemical expansion by controlling charge localization: In Situ X-ray diffraction and dilatometric study of $(\text{La},\text{Sr})(\text{Ga},\text{Ni})\text{O}_{3-\delta}$ perovskite," *Journal of Materials Chemistry A* 2 (2014) 18906-18916
- ³¹ D. Marrocchelli, S. R. Bishop, H. L. Tuller, G. W. Watson, and B. Yildiz, "Charge localization increases chemical expansion in cerium-based oxides," *Physical Chemistry Chemical Physics*, 14, 12070-12074 (2012)
- ³² N.H. Perry, J.E. Thomas, D. Marrocchelli, S.R. Bishop, and H.L. Tuller, "Isolating the role of charge localization in chemical expansion: $(\text{La},\text{Sr})(\text{Ga},\text{Ni})\text{O}_{3-x}$ Case Study," *ECS Transactions*, v. 57, no. 1, pgs. 1879-1884 (2013)
- ³³ J. Mizusaki, T. Sasamoto, W.R. Cannon, and H.K. Bowen, "Electronic conductivity, Seebeck coefficient, and defect structure of $\text{La}_{1-x}\text{Sr}_x\text{FeO}_3$ ($x = 0.1, 0.25$)" *J. Am. Ceram. Soc.* 66 (1983) 247-252
- ³⁴ D. Marrocchelli, N.H. Perry, and S.R. Bishop, "Understanding chemical expansion in perovskite-structured oxides," (under review)
- ³⁵ R.D. Shannon, "Revised effective ionic radii and systematic studies of interatomic distances in halides and chalcogenides," *Acta Cryst.* A32 751-767 (1976)
- ³⁶ M. Vračar, A. Kuzmin, R. Merkle, J. Purans, E.A. Kotomin, J. Maier, and O. Mathon, "Jahn-Teller distortion around Fe^{4+} in $\text{Sr}(\text{Fe}_x\text{Ti}_{1-x})\text{O}_{3-\delta}$ from X-ray absorption spectroscopy, X-ray diffraction, and vibrational spectroscopy," *Physical Review B* 76 (2007) 174107, 12pp
- ³⁷ S.R. Bishop, K.L. Duncan, and E.D. Wachsman, "Surface and bulk oxygen non-stoichiometry and bulk chemical expansion in gadolinium-doped cerium oxide," *Acta Materialia* 57 (2009) 3596-3605
- ³⁸ S.R. Bishop, T. Nakamura, and K. Amezawa, "Chemically-induced expansion of $\text{Zr}_{0.2}\text{Ce}_{0.8}\text{O}_{2-\delta}$," *Solid State Ionics* 261 (2014) 1-4
- ³⁹ S. Omar and J.C. Nino, "Consistency in the chemical expansion of fluorites: A thermal revision of the doped ceria," *Acta Materialia* 61 [14] (2013) 5406-5413
- ⁴⁰ C. Greaves and R.A. Buker, "The defect structure of $\text{Sr}_2\text{FeTiO}_{6-x}$," *Materials Research Bulletin* 21 [7] (1986) 823-833
- ⁴¹ J. Rodriguez, P.A. Pereda, M. Vallet, J.G. Calbet, and J. Tejada, "Mossbauer study of vacancy ordering in the system $\text{SrTi}_{1-x}\text{Fe}_x\text{O}_{3-y}$ ($0.5 \leq x \leq 0.70$)," *Materials Research Bulletin* 21 [3] (1986) 255-263

-
- ⁴² P. Adler and S. Eriksson, "Structural properties, Mossbauer spectra, and magnetism of perovskite-type oxides $\text{SrFe}_{1-x}\text{Ti}_x\text{O}_{3-y}$," *Zeitschrift für anorganische und allgemeine chemie* 626 [1] (2000) 118-124
- ⁴³ D. Marrocchelli, S.R. Bishop, and J. Kilner, "Chemical expansion and its dependence on the host cation radius," *Journal of Materials Chemistry A*, 1 [26] (2013) 7637-7680
- ⁴⁴ V.V. Kharton, A.A. Yaremchenko, M.V. Patrakeev, E.N. Naumovich, F.M.B. Marques, "Thermal and chemical induced expansion of $\text{La}_{0.3}\text{Sr}_{0.7}(\text{Fe,Ga})\text{O}_{3-\delta}$ ceramics," *Journal of the European Ceramic Society* 23 (2003) 1417-26
- ⁴⁵ M. Ram and Y. Tsur, "Eliminating chemical effects from thermal expansion coefficient measurements," *J. Electroceram.* 22 (2009) 120-124
- ⁴⁶ M. Kakihana and M. Yoshimura, "Synthesis and characteristics of complex multicomponent oxides prepared by polymer complex method," *Bull. Chem. Soc. Jpn.* 1999, 72, 1427-1443
- ⁴⁷ J.B. Wachtman, Jr., T.G. Scuderi, and G.W. Cleek, "Linear thermal expansion of aluminum oxide and thorium oxide from 100° to 1100°K," *J. Am. Ceram. Soc.* 45 [7] (1962) 319-323